Modeling the Rheology of Concentrated AB/AB_2 Hyperbranched Polymeric Systems

A. T. Lee and A. J. McHugh*

Department of Chemical Engineering, University of Illinois, Urbana, Illinois 61801

Received August 9, 2001; Revised Manuscript Received September 28, 2001

ABSTRACT: The approach of Blackwell et al. is used to model the rheology of concentrated hyperbranched polymeric systems. Model predictions for a poly(ether imide) hyperbranched system are in good quantitative agreement with the experimentally observed behavior of AB/AB_2 copolymers. The poly(ether imide)s are especially suitable for studies of entangled dynamics because of their low entanglement molecular weight. A 3−4 orders of magnitude rise in the zero shear viscosity is observed as the mole fraction of linear segments is varied from 0 to 1. The average mass of segments between branch points is the most significant architectural parameter that affects the rheology of these systems.

Introduction

The rheological properties of polymer melts are known to depend strongly on three underlying molecular structure parameters: molecular weight, molecular weight distribution, and molecular architecture (branching). In recent years, there has been considerable interest in the development of models relating the melt rheology of a polymer to its molecular architecture.[1,2] It is desirable to be able to predict the rheological properties given a molecular architecture and, possibly, vice versa.

Branched polymers can be broadly classified as stars, long-chain branched polymers, and dendritic polymers. The star polymer architecture is obtained by the simple introduction of a single branch point in a linear chain. Long-chain branched polymers typically comprise a single long backbone chain with several sidearms. The arms themselves have very little additional branching. Dendritic polymers have the most complex architecture of the three and consist of a layer upon layer, treelike topology.

Dendritic materials can be further classified as perfect dendrimers and hyperbranched polymers (HBPs). While their precise functionality and end-group multiplicity lend perfect dendrimers several attractive properties such as high solubility and low viscosities, their systematic step-by-step synthesis is expensive, and large-scale industrial synthesis is not considered viable.

Our own recent research has focused on HBPs. While these molecules do not have the well-defined monodisperse structure of perfect dendrimers, they are much more rapidly and economically synthesized by a single-step polycondensation between AB_x ($x \geq 2$) monomers containing one reactive group (A) and x reactive groups (B) of another type. Moreover, they possess a layer upon layer topology similar to perfect dendrimers and are known to exhibit similar rheological properties.[3] Literature reviews of rheological studies performed by other research groups on both perfect dendrimers and hyperbranched polymers may be found in our earlier publications.[3−7] Recently, in an attempt to further understand the effects of molecular architecture on rheology, a series of AB/AB_2 poly(ether imide) copolymers have been synthesized and characterized in our laboratory.[4] The molecular weights of these samples have been maintained almost constant, while incremental architectural changes have been achieved by varying the ratio of AB to AB_2 monomer units. The primary finding has been that a transition from dendrimer-like properties (low viscosity) to linear-chain-like properties (high viscosity coupled with nonlinear viscoelastic effects) occurs when the mole fraction of linear segment (AB) units in the starting monomer mixture exceeds 0.75. This result has been observed for both dilute and concentrated solutions[5] in NMP (*N*-methylpyrrolidinone). Nonequilibrium Brownian dynamics calculations have been performed on a series of constant molecular weight hyperbranched systems with varying amounts of linear units, utilizing a bead−spring−trumbbell model.[6] Simulation results are in good agreement with dilute solution data. The transition in properties is associated with a marked rise in the mean-squared radius of gyration, when the mole fraction of AB units exceeds 0.75. The poly(ether imide)s are also characterized by low entanglement molecular weights, which lead to their displaying entanglement effects at high concentrations. Currently, an understanding of the rheological behavior of these constant molecular weight AB/AB_2 copolymers in the concentrated regime is lacking.

The "tube model", originated by de Gennes[8] and developed into a full constitutive theory by Doi and Edwards,[9] has been the most successful and widely accepted theory for polymer molecules in the entangled state. Later developments led to theories for more complicated architectures such as star polymers, combs, and H-polymers. A good review of the history of tube theories for complex architectures can be found elsewhere.[1] Most recently, Blackwell et al.[10] have provided a general treatment of the entangled dynamics of symmetric treelike molecules with any number of layers. The stretch and orientation in different sections of the molecule were shown to be coupled, and a novel constitutive equation set was derived. In this paper we wish to demonstrate the application of the Blackwell method to model the rheological behavior of the AB/AB_2 copolymers we have observed in the concentrated state.[5] Even though hyperbranched polymers are not perfectly branched symmetric structures and are usually a mixture of several different structural isomers, we assume

* To whom correspondence should be addressed.

10.1021/ma011430s CCC: $20.00
Published on Web 11/08/2001

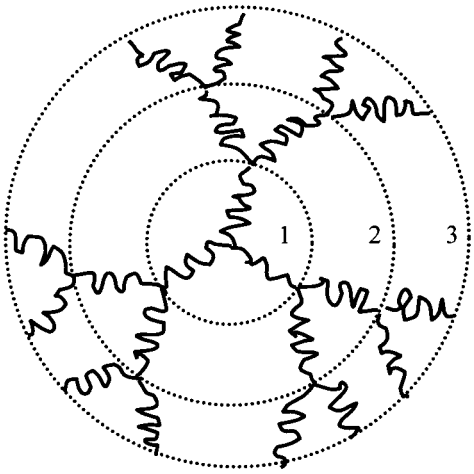

Figure 1. Schematic of a three-layer treelike molecule.

here that, on an average, they may be represented by symmetrically branched molecules. In the next section, we briefly describe the theoretical methodology involved in the calculation of the various linear and nonlinear rheological properties. We also describe the modeling procedure and how the molecular variables relate to the model parameters. This is followed by a presentation and discussion of the key results and model predictions.

Theory and Methods

Rheology of Treelike Polymers. The origins of the various elements of the model are fully discussed in the paper by Blackwell et al.[10] and the references therein. Here, we summarize only the key assumptions and equations used. A schematic of a three-layer tree is shown in Figure 1. The sections of chain in the molecule can be divided among layers or zones. All chain segments in each layer have the same mass and are connected to a fixed number of other chains. The layers are numbered from the center of the molecule to the free ends, so that the outermost arms form layer n and the layer nearest the center is 1. Arc coordinates x_i are defined from the centermost end of each segment toward the free end, so that $x_i = 0$ at the innermost end of each segment in layer i and $x_i = 1$ at the outermost end. Another coordinate y runs from the center of the molecule to the free end so that, in layer i, $y = (i - 1) + x_i$. The number of arms attached to branch points in each layer is denoted by q_i. As there has to be a branch point at the center of the molecule, q_1 is always greater than 2. Arm molecular weights in each layer, M_i, are scaled by the entanglement molecular weight, M_e, to yield dimensionless arm lengths, $s_i = M_i/M_e$. The treelike topology is specified by the values of q_i and s_i. In addition, only two parameters need to be specified: the plateau modulus, G_0, and the Rouse time of an entanglement segment, τ_e. Both parameters are independent of topology and depend only on the chemical structure of the polymer. They may be obtained from experiments on linear polymers of the same chemistry. τ_e is given by

$$\tau_e = \frac{\zeta N_e^2 b^2}{3\pi^2 kT} \tag{1}$$

where ζ is the monomeric friction coefficient, N_e is the number of monomers between entanglements, k is the Boltzmann constant, T is temperature, and b is the length of a monomeric unit.

The orientation of the primitive chains relaxes by the segments fluctuating about their equilibrium length. Incorporating the effects of dynamic dilution gives the energy barrier to relaxing fluctuations as[10]

$$U_i(x_i) = \frac{\nu s_i kT}{\beta(\beta+1)\phi_i^2}(u_i^{\beta+1} - (u_{i-1} + x_i\phi_i)^\beta(u_i + \beta\phi_i(1 - x_i))) \tag{2}$$

ν is the Doi−Edwards parameter and is taken to be 15/4. α and β are dilution scaling parameters[11] and are given by $\alpha = {}^4/_3$ and $\beta = \alpha + 1$. The tube diameter scales with the unrelaxed fraction in each layer as $a(u_i) = a_0 u_i^{-\alpha/2}$. ϕ_i is the mass fraction of a layer, and u_i is the fraction of unrelaxed polymer segments.

$\tau_i(x_i)$ is defined as the relaxation time of the chain at arc coordinate x_i. Relaxation occurs first in the free diffusion time, $\tau_{E,i}(x_i)$, and later by dynamic dilution, $\tau_{L,i}(x_i)$. The following crossover formula is used to evaluate the overall relaxation time[12]

$$\tau_i(x_i) = \tau_{i+1}(0) + \frac{\tau_{E,i}(x_i)e^{U_i(x_i)/kT}}{1 + \frac{\tau_{E,i}(x_i)}{\tau_{L,i}(x_i)}e^{U_i(x_i)/kT}} \tag{3}$$

The relaxation modulus $G(t)$ depends only on the relaxation time and is given by

$$G(t) = G_0\int_0^n dy\, e^{-t/\tau(y)}\frac{d}{dy}\Phi(y)^\beta \tag{4}$$

where Φ is the fraction of unrelaxed chains when the relaxation has reached x_i, and G_0 is the plateau modulus. The storage and loss moduli, G' and G'', are obtained by evaluating the Fourier sine and cosine transforms of $G(t)$, respectively. The zero shear viscosity is found by integrating $G(t)$ over time.

$$\eta_0 = G_0\int_0^n dy\, \tau(y)\frac{d}{dy}\Phi(y)^\beta \tag{5}$$

The stress from each segment depends on the molecular stretch ratio, λ_i, and the orientation tensor given by the second moment of the primitive chain tangent vectors, $\mathbf{S}_i = \langle \mathbf{u}_i\mathbf{u}_i\rangle$. At equilibrium, all segments have a stretch ratio of unity and are isotropically oriented. $\lambda^2\mathbf{S}$ are counted from each point along the chain and multiplied by the appropriate dilution factor to yield the stress tensor

$$\sigma(\mathbf{K},t) = \nu G_0\sum_{i=1}^{n}\lambda_i^2(\mathbf{K},t)\int_0^1 dx_i\, S_i(\mathbf{K},x_i,t)\frac{d}{dx_i}\Phi_i(x_i)^\beta \tag{6}$$

where $\mathbf{K}$ is the transpose of the velocity gradient tensor. The PDE's[10] for the evolution of the segmental stretch, λ_i, and orientation, $\mathbf{S}_i$, are solved numerically using second-order Runge−Kutta routines. The shear and extensional viscosities and the first normal stress coefficient are calculated using their standard definitions.

Modeling HBP's as Treelike Structures. While the methodology described in this section is valid for hyperbranched molecules of any chemistry, we specialize it for the poly(ether imide) (PEI) HBP system studied.[4,5] Monomeric poly(ether imide) can be either

monofunctional (AB) or bifunctional (AB_2). The AB unit is *N*-[3-(*tert*-butyldimethylsilyloxy)phenyl-4-fluorophthalimide] and the AB_2 unit, which has an additional reactive *tert*-butyldimethylsilyloxy (TBS) group, is *N*-[3,5-di(*tert*-butyldimethylsilyloxy)phenyl-4-fluorophthalimide]. During polymerization, the fluorine reacts with the hydrogen on TBS, yielding hydrogen fluoride and linking two monomeric units. Molecules with varying amounts of branching are obtained by changing the relative amounts of AB and AB_2 reactants initially in the reaction mixture.

Once polymerized, the AB_2 units can exist in three states: linear, dendritic, and terminal, which we denote by *L*, *D*, and *T*, respectively. Linear units are those in which only one of the B groups reacts. In the dendritic units, both B's react, giving rise to a branch point. Terminal units occur at the chain ends, and both their B groups are unreacted. Similarly, the AB units can exist in two states: linear and terminal, denoted by L_l and T_l. For PEI, the *D*, *L*, and *T* units have molecular weights of 480, 481, and 482, g/mol respectively, while the L_l and T_l units have weights of 350 and 351 g/mol, respectively.

If one assumes that all B groups possess the same reactivity, regardless of whether they belong to AB or AB_2 monomers, and if one assumes that all initial monomer units react completely, it is possible to obtain expressions[13] for the mole fractions (or probability distribution) of *D*, *L*, *T*, L_l, and T_l units:

$$p(D) = \frac{r+1}{(r+2)^2} \tag{7}$$

$$p(L) = \left(\frac{2}{r+2}\right)\left(1 - \frac{r+1}{r+2}\right) \tag{8}$$

$$p(T) = \left(\frac{1}{r+1}\right)\left(1 - \frac{r+1}{r+2}\right)^2 \tag{9}$$

$$p(L_l) = \frac{r}{r+2} \tag{10}$$

$$p(T_l) = \left(\frac{r}{r+1}\right)\left(1 - \frac{r+1}{r+2}\right) \tag{11}$$

In these expressions, *r* is the mole ratio of AB to AB_2 monomers:

$$r = \frac{x_1}{x_2} \tag{12}$$

where x_1 and x_2 are the mole fractions of AB and AB_2 units, respectively.

If the total molecular weight of the polymer, M_{tot}, is known, then the total moles of monomer units in the molecule, N_{tot}, may be calculated utilizing the expression

$$M_{tot} = (p(D)N_{tot} \times 480) + (p(L)N_{tot} \times 481) + (p(T)N_{tot} \times 482) + (p(L_l)N_{tot} \times 350) + (p(T_l)N_{tot} \times 351) \tag{13}$$

and the moles of the individual units N_L, N_D, N_T, N_{Ll}, and N_{Tl} may be evaluated.

The total mass of the molecule is distributed among segments connecting two branch points or a branch point and a free end. The average segmental mass is given by

Table 1

mole fraction of AB units, x_{AB}	avg segmental mass, M_{seg} (g/mol)	no. of layers	total mol wt (g/mol)	exptl[a] mol wt (g/mol)
0	962	5	89 466	73 000
0.25	915	5	85 112	80 625
0.5	935	5	86 944	72 600
0.75	1196	4	53 824	60 600
0.8	1354	4	60 944	71 735
0.825	1471	4	66 198	77 850
0.85	1630	4	73 329	60 800
0.875	1855	4	83 465	71 900
0.9	2197	4	98 854	80 000
0.925	2772	3	58 215	84 050
0.95	3931	3	82 550	101 850

[a] Average of molecular weights determined by the TriSEC method and the SLLS method.[5]

$$M_{seg} = \frac{M_{tot}}{N_D + N_T + N_{Tl}} \tag{14}$$

If the chemical kinetics are random, then the dendritic units, *D*, are on average distributed among the various layers, in a 2^i manner; i.e., the *i*th layer possesses twice as many branch points as the $(i-1)$th layer, just as in a Cayley tree. We further assume that the terminal units are distributed predominantly in the outermost layer. Thus, the AB/AB_2 hyperbranched polymers are modeled as Cayley trees with identical segments of mass, M_{seg}. For a given value of M_{seg}, 3-, 4-, 5-, and 6-layer Cayley tree structures, with $q_1 = 3$ and $q_2, q_3 \ldots = 2$, are generated, and the structure whose total molecular weight is closest to the experimental M_{tot} is chosen.

Results and Discussion

A series of architectures with incrementally varying mole fractions of AB units have been studied. The average segment mass, number of layers, and theoretical and experimental molecular weights for each structure are listed in Table 1. The counterintuitive initial drop in the average segmental mass, when the mole fraction of linear units is increased, is due to the mismatch in the molecular weights of the AB and AB_2 type units. However, this effect is significant only at the low x_{AB} values, and M_{seg} increases as expected, beyond $x_{AB} = 0.25$.

To evaluate the linear and nonlinear rheological properties, values for the plateau modulus, G_0, entanglement molecular weight, M_e, and the Rouse time of entangled segments, τ_e, are required. M_e is essentially independent of temperature, while G_0 is linearly dependent on temperature and τ_e is a strong function of temperature. Biddlestone et al.[14] have measured a plateau modulus of 9 MPa for linear poly(ether imide) in the melt state at 220 °C. The density[14] of PEI at the temperature is 1.27 g/cm^3. The entanglement molecular weight is related to G_0 through

$$M_e = \frac{\rho R T}{G_0} \tag{15}$$

which yields a value of 578 g/mol.

Experimental data[5] are available for entangled AB/AB_2 PEI systems at a concentration of 0.83 g/mL and a temperature of 5 °C. To make comparisons with the available data, model parameters need to be scaled to

the new concentration and temperature. According to Ferry,[15] the entanglement molecular weight is proportional to $(c/\rho)^{-1}$ and the plateau modulus scales as $(c/\rho)^2$, where ρ is the melt density and c is the new concentration. Following this procedure yields $M_e = 884$ g/mol and $G_0 = 2.17 \times 10^6$ Pa, which are the parameter values used in all our calculations. The length of a monomer unit is estimated from bond length data to be[14] 3.44×10^{-9} m. However, an accurate estimate of the monomeric friction coefficient at 5 °C is not available. Thus, τ_e is used as an adjustable parameter to best fit the data. A value of 4.43×10^{-6} s for τ_e is found to be optimal and used in all our calculations. According to eq 1, this corresponds to a monomeric friction coefficient value of $\zeta = 6.67 \times 10^{-9}$ N s/m. We should note that Colby and Rubinstein[11] suggest a dilution exponent of $^4/_3$ for the concentration scaling of M_e. However, an appropriate change in τ_e would lead to the same quantitative predictions.

The hierarchy of relaxation times for each structure is evaluated first. Before further calculations of rheological properties, it is necessary to check the validity of entangled dynamics, which we have assumed. We utilize the condition proposed by Milner et al.,[16] that the rate of tube dilation must always be less than the rate of retraction, for entanglements to be important. If the dilution occurs rapidly compared to the relaxation of the chain, then "Rouse tube" dynamics and not entangled dynamics, provide the fastest relaxation mechanism. Following Milner et al.,[16] we compare the expressions for constraint release through each mechanism

$$\left(\frac{d\Phi}{dt}\right)_{\text{Rouse}}(y) = -\frac{\Phi(y)}{2\alpha\tau(y)} \tag{16}$$

$$\left(\frac{d\Phi}{dt}\right)_{\text{entangled}}(y) = \frac{d\Phi}{dy}\frac{dy}{dt} = \frac{d\Phi}{dy}\Big/\frac{d\tau(y)}{dy} \tag{17}$$

The constraint release rates for the $x_{AB} = 0.95$ polymer are plotted in Figure 2a. Clearly the dynamic dilution occurs more slowly than the Rouse tube motion across the entire molecule, and entangled dynamics are valid. The singularities near the intermediate branch points are an artifact of the assumption of free diffusion at the large x ends of the segments and may be ignored. Similarly, for all the structures with $x_{AB} > 0.5$, the entangled dynamics are found to be valid across almost the entire range of relaxation times(not shown). However, for the three highly branched molecules with x_{AB} values less than and including 0.5, the constraint release rate of entangled dynamics is found to be faster than that of Rouse motion, in the innermost layers. This phenomenon is known as[10] a "disentanglement transition", and beyond the crossover point, the assumed entangled dynamics are not valid. Figure 2b shows the entangled and Rouse rates for the $x_{AB} = 0$ molecule, illustrating that the transition occurs between the second and first layers. However, since the majority of the molecular weight is distributed among the outer layers, the contribution of the dynamics of the innermost layers to the overall rheology is small. Thus, the crossover may be reasonably neglected.

The zero shear viscosities are evaluated by integrating the relaxation spectrum over all the layers of the molecule, utilizing eq 5. Figure 3a depicts the model

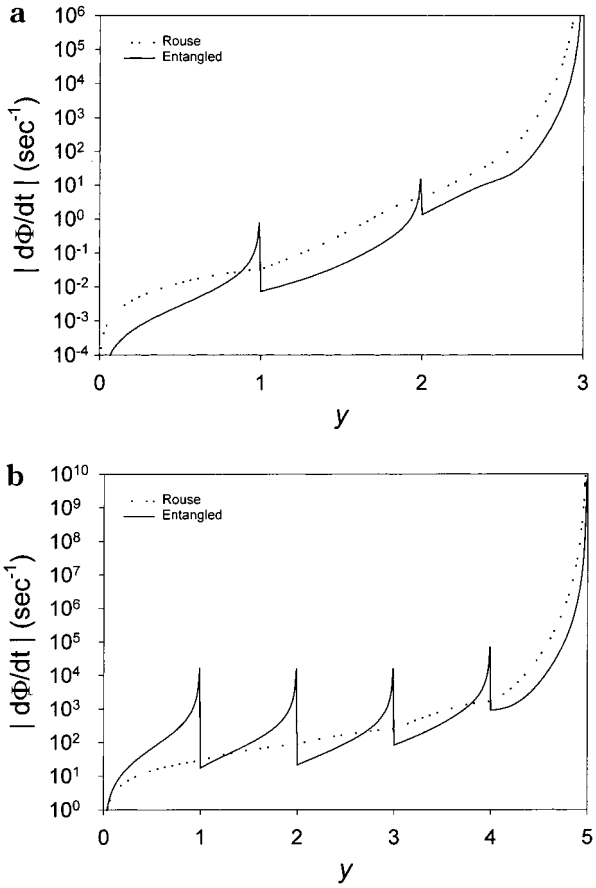

Figure 2. (a) Entangled and Rouse rates of constraint release for the $x_{AB} = 0.95$ polymer. (b) Entangled and Rouse rates of constraint release for the $x_{AB} = 0$ polymer.

predictions for the zero shear viscosities of the various architectures, plotted alongside the experimental results. The zero-shear viscosity for the completely linear chain ($x_{AB} = 1$) is calculated using the reptation model, $\eta_0 = (\pi^2/12)G_0\tau_d$, where τ_d is the characteristic reptation time, given by $\tau_d = \zeta N^3 b^4/(\pi^2 k_B T a^2)$, and the average tube diameter "a" is given by $a^2 = 4M_e N b^2/5M$.

Unlike in the dilute solution, where a rise in viscosity of less than an order of magnitude is observed,[4−6] a stronger increase of 3−4 orders of magnitude is observed in the entangled state, as x_{AB} is varied from 0 to 1. This behavior is better understood by analyzing the expression for the zero shear viscosity in eq 5. The viscosity is obtained by integrating the relaxation time $\tau(y)$ over all the layers. The primary architectural variable that changes when x_{AB} increases is the average segmental mass. The early time τ_E for the outermost layer scales as s^4, where s is the dimensionless segment mass. Following the approximation of Milner and McLeish,[12] the late time τ_L is found to scale as $s^3 e^U/U$, where U is the energy barrier to the relaxation. Now, from eq 2, U is directly proportional to the segment mass, s, with a proportionality constant of the order of 1. Thus, the leading term in the expression for $\tau(y)$ scales as $s^2 e^s$. The segmental mass of the $x_{AB} = 0.95$ structure is roughly 4 times that of the $x_{AB} = 0$ structure, which corresponds to an $s^2 e^s$ value of 874. Hence, the viscosity of the $x_{AB} = 0.95$ molecule is roughly 3 orders of magnitude higher.

It is also interesting to note that the average segmental mass does not depend on the total molecular weight for these AB/AB$_2$ systems. All three quantities in the denominator of eq 14 are linearly related to the

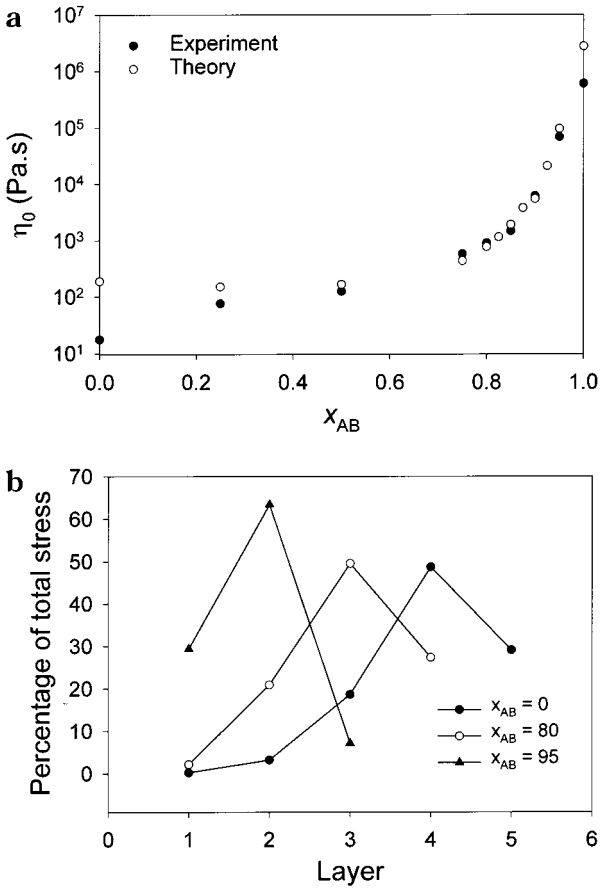

Figure 3. (a) Model predictions of zero shear viscosity plotted against starting mole fraction of AB units. Model parameters used are $G_0 = 2.17 \times 10^6$ Pa, $M_e = 884$ g/mol, and $\tau_e = 4.43 \times 10^{-6}$ s. Closed symbols represent the experimental data (concentration = 0.83 g/mL and temperature = 5 °C) of Sendijarevic et al.[5] (b) Fractional contribution of each layer to the viscosity integral.

total molecular weight. Thus, M_{tot} cancels out, leaving the segmental mass a function of architecture (x_{AB}) alone.

The molecules with x_{AB} values up to 0.5 have average segmental masses ranging from 915 to 962 g/mol. The calculated entanglement molecular weight is 884 g/mol. Thus, even though the model suggests that entanglements are important in the outer layers of these structures, it is questionable how much of a role entanglements actually play in their experimentally observed rheology. That the molecules are in an overlapped rather than entangled state is a possible explanation for the deviations of model predictions from the experimental data at the lower x_{AB} values.

The small deviation between the Doi−Edwards prediction and the experimental value at $x_{AB} = 1$ could be due to effects of polydispersity and contour length fluctuations. However, these issues are not addressed in this study.

In Figure 3b, the relative contributions of the dynamics of each layer to the total viscosity are plotted for the $x_{AB} = 95$, $x_{AB} = 80$, and $x_{AB} = 0$ molecules, which are representative of 3-, 4-, and 5-layer structures, respectively. While the outermost layer has the highest mass fraction of segments, it is also comprised purely of free ends, which relax rapidly on their bare Rouse time scales. The layer just inside the outermost layer is the one with the largest mass fraction of segments which

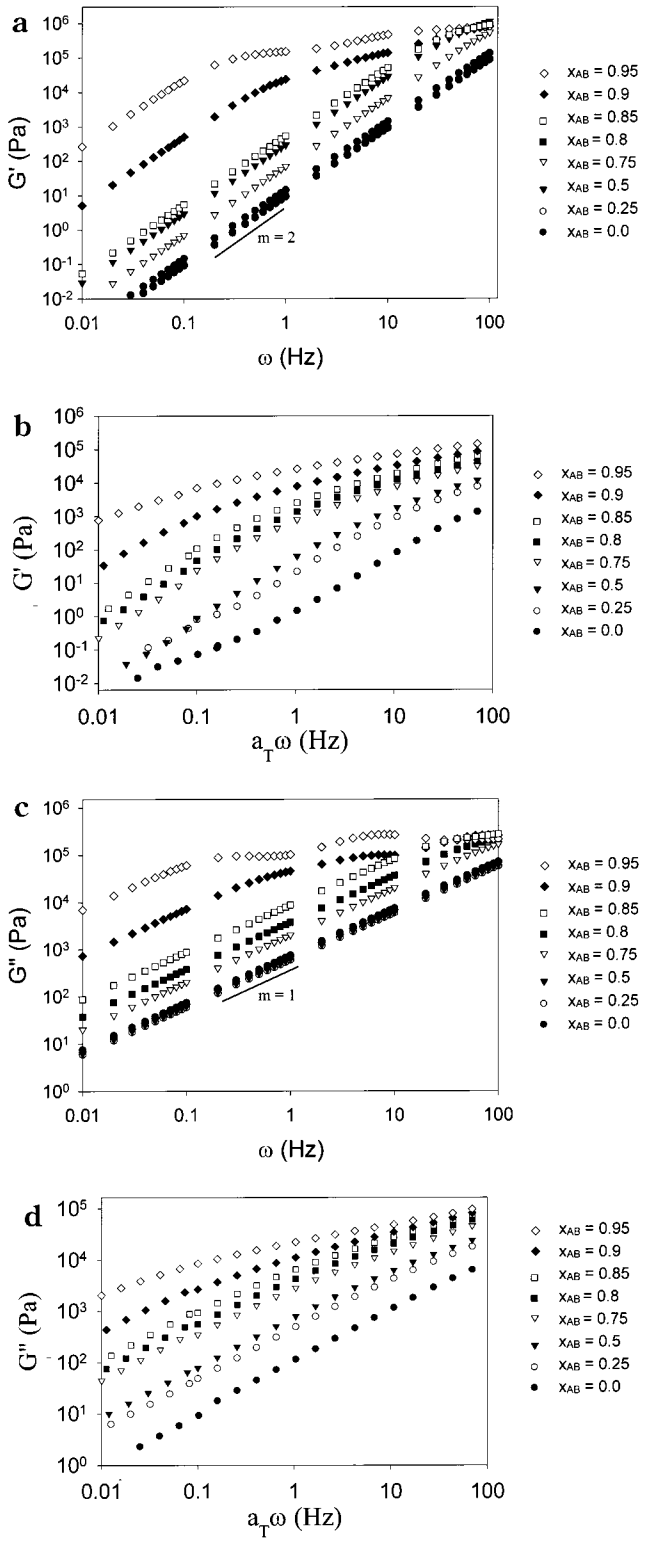

Figure 4. (a) Model predictions for the storage moduli. Model parameters used are the same as in Figure 3a. (b) Experimentally observed storage moduli for 0.83 g/mL system at $T_{ref} = 5$ °C, from Sendijarevic et al.[5] The data are shifted according to the temperature shift factor a_T. (c) Model predictions for the loss moduli. Model parameters used are the same as in Figure 3a. (d) Experimentally observed loss moduli for 0.83 g/mL system at $T_{ref} = 5$ °C, from Sendijarevic et al.[5] The data are shifted according to the temperature shift factor a_T.

are trapped between two branch points. Thus, it is the most dominant contributor to the overall stress. As one moves toward the center of the molecule, the mass fraction in the layers decrease exponentially, which, in

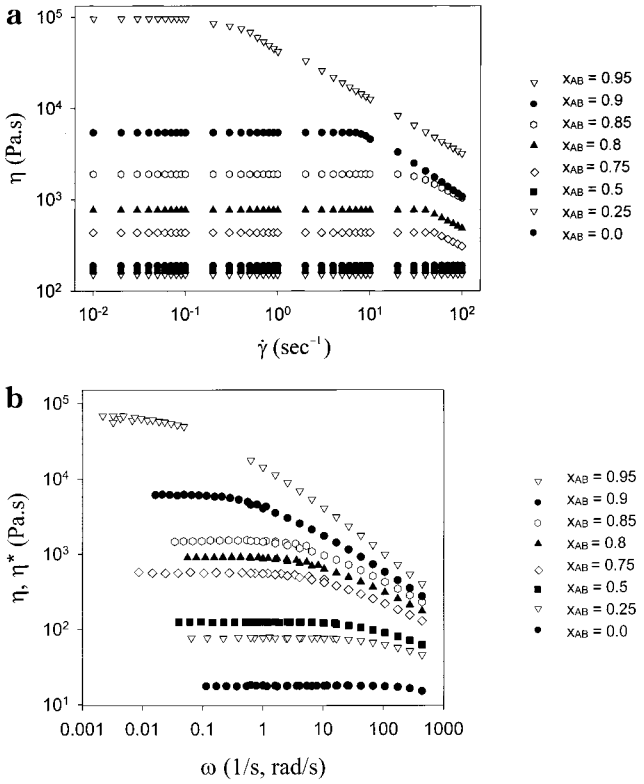

Figure 5. (a) Model shear thinning behavior. Model parameters used are the same as in Figure 3a. (b) Experimentally observed[5] shear thinning behavior at a concentration of 0.83 g/mL and temperature of 5 °C.

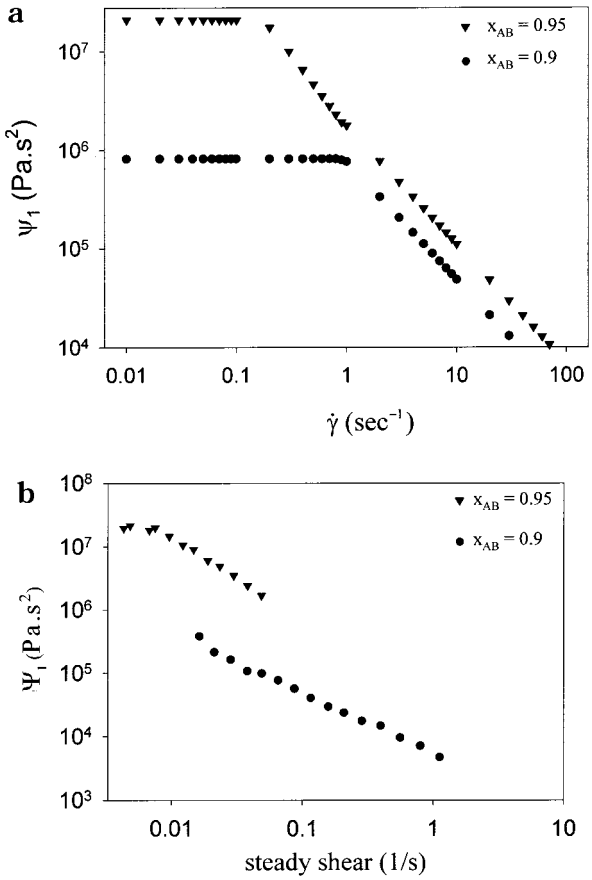

Figure 6. (a) Model predictions for the first normal stress coefficients. Same model parameters as in Figure 3a. (b) Experimentally measured first normal stress coefficients at a concentration of 0.83 g/mL and temperature of 5 °C.

combination with the effects of dynamic dilution, causes them to have less significant effects on the rheology.

Model predictions and experimental data for the storage and loss moduli are depicted in Figure 4a−d. Two distinct "humps" are observed in the predicted G' of the $x_{AB} = 0.95$ molecule. The humps correspond to the two innermost layers of the molecule and are even more pronounced in the G'' plot. Similarly, the $x_{AB} = 0.9$ structure displays a single hump. According to previous studies of H-polymers[17] and Cayley trees,[10] the dynamic moduli are expected to display humps corresponding to each layer of the molecule. One would have to sample much higher frequencies to observe all the humps in our systems. The moduli for the structures with $x_{AB} < 0.9$ correspond to their innermost layer in this frequency range, and a Rouse-like dependence of $G' \sim \omega^2$ and $G'' \sim \omega$ is exhibited. The experimental data do not exhibit humps because of the wide polydispersity and the number of structural isomers. However, it is the experimental high x_{AB} molecules which exhibit viscoelastic effects and a tendency to plateau. The experimentally observed Rousean behavior at the lower frequencies and the overall quantitative agreement with the model predictions are notable.We next examine the nonlinear rheological response under shear flow. The viscosities at various shear rates for each structure are plotted in Figure 5a. For the range of shear rates considered, the inner two layers of the $x_{AB} = 0.95$ molecule are active, and for the rest of the molecules, only the innermost layer is active. The innermost segments follow the established Doi−Edwards form at the low shear rates. When the shear rates exceed $\tau(1)^{-1}$, where $\tau(1)$ is the relaxation time at the interface between layers 1 and 2, segments in layer 1 get "advected" on to those in layer 2. The advected tube from segment 1 reduces the nonlinear orientation[10] of segment 2. This is evident in Figure 5a, for the $x_{AB} = 0.95$ structure, whose $\tau(1)$ is around 1 s. Beyond a shear rate of 1 s^{-1}, tube advection sets in and a weaker shear thinning slope is observed. For the remaining structures, $\tau(1)$ lies outside the range of shear rates considered and no change in slope is observed. For the three lowest x_{AB} structures, the relaxation time of the innermost layer is of the order of 10^{-4} s, and a shear rate of 10 000 s^{-1} would be required just to observe the onset of Doi−Edwards type shear thinning. The experimentally observed viscosities are shown in Figure 5b. Even though one does not observe any marked changes in slope or other effects of coupling between layers, it is still interesting to note the earlier onsets of shear thinning and larger relaxation times of the high x_{AB} molecules. The experimental shear thinning slopes range from −0.18 to −0.76 as x_{AB} ranges from 0 to 0.95, while the theoretical slopes vary from 0 to −0.7. Experimentally, the onset of shear thinning is found to occur at shear rates of 110 s^{-1} for $x_{AB} = 0$ and 0.02 s^{-1} for the $x_{AB} = 0.95$ sample. In the range of shear rates studied, the model molecules do not exhibit shear thinning for x_{AB} values up to 0.5, while the onset of shear thinning occurs at a shear rate of 0.1 s^{-1} for the $x_{AB} = 0.95$ molecule.

In Figure 6a,b the predicted and experimental first normal stress coefficients are depicted for the $x_{AB} = 0.95$ and $x_{AB} = 0.9$ structures. As in the case of the viscosities, the onset of shear thinning corresponds with the characteristic relaxation time of the innermost layer. However, the magnitudes of shear thinning are higher

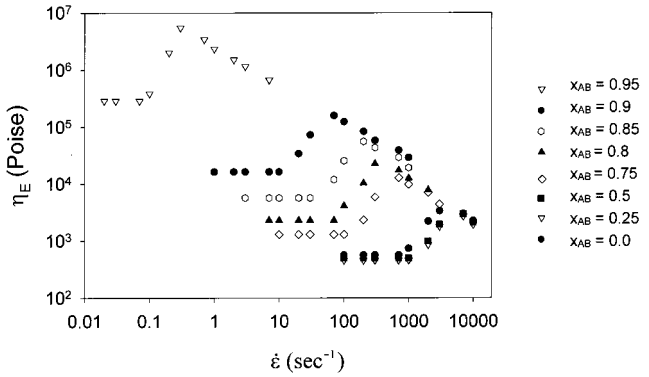

Figure 7. Model predictions for uniaxial extensional flow. Same model parameters as in Figure 3a.

compared to the viscosities, with both structures showing asymptotic slopes of around −1.3. Experimentally, asymptotic slopes closer to −1 are observed, and there is good quantitative agreement between the model and experimental zero shear values.

Predicted uniaxial extensional viscosities for each of the structures are shown in Figure 7. As in previous studies of pom-pom polymers[2] and treelike polymers,[10] extensional hardening is observed, which is followed by an almost linear drop in viscosity. The strain hardening is caused by the rapid stretch of the innermost segments to their maximum value. Once the maximum value is reached, advection pushes the aligned tube out from segment 1 onto segment 2. Unlike shear flow, tube advection causes a rapid rise in the alignment of segment 2, which leads to the ensuing extension thinning behavior. However, stretching of segment 2 increases the priority of segment 1, giving it a time-dependent priority and allowing it to stretch further. With a sufficiently large number of data points, one must be able to see tiny peaks associated with segments in each of the outer layers reaching their maximum priority. However, only the main peaks associated with the innermost layers are shown in Figure 7. Unfortunately, there are no experimental data available for these AB/AB_2 polymers under uniaxial extensional flow.

In summary, because of their lower branching and the consequent higher average segment mass, the high-x_{AB} molecules possess inner layers with much higher relaxation times compared to those of the low-x_{AB} structures. As a result, they have a higher tendency to exhibit nonlinear viscoelastic behavior, such as shear thinning, extension hardening, and plateauing of moduli in the experimentally relevant frequency range.

Conclusions

In this paper, we have modeled the entangled dynamics of hyperbranched polymers, following the procedure proposed by Blackwell et al.[10] The architecture has been incrementally varied for a series of AB/AB_2 type copolymers. The average mass of the segments between branch points is an important parameter which affects the rheology. The molecules with higher mole fractions of AB units have larger segmental masses and have a greater tendency to exhibit nonlinear viscoelastic effects. Model predictions are in good quantitative agreement with the experimental data for the poly(ether imide) hyperbranched systems in the entangled state. Together with our previous Brownian dynamics study,[6] we now have a reasonable quantitative understanding of the rheological behavior of the AB/AB_2 copolymers, in the two extreme states of dilute solution and entangled concentrated solution.

Acknowledgment. This work has been supported under a grant from the U.S. Army Research Office under Contract/Grant DAAG55-97-0126.

References and Notes

(1) McLeish, T. C. B.; Milner, S. T. *Adv. Polym. Sci.* **1999**, *143*, 195.
(2) McLeish, T. C. B.; Larson, R. G. *J. Rheol.* **1998**, *42*, 81.
(3) Sendijarevic, I.; McHugh, A. J. *Macromolecules* **2000**, *33*, 590.
(4) Markoski, L. J.; Moore, J. S.; Sendijarevic, I.; McHugh, A. J. *Macromolecules* **2001**, *34*, 2695.
(5) Sendijarevic, I.; McHugh, A. J.; Markoski, L. J.; Moore, J. S. *J. Rheol.* **2001**, *45*, 1245.
(6) Lee, A. T.; McHugh, A. J. *Macromolecules* **2001**, *34*, 7127.
(7) Lee, A. T.; McHugh, A. J. *Macromol. Theory Simul.* **2001**, *10*, 244.
(8) de Gennes, P. G. *J. Chem. Phys.* **1971**, *55*, 572.
(9) Doi, M.; Edwards, S. F. *The Theory of Polymer Dynamics*; Oxford: New York, 1989.
(10) Blackwell, R. J.; Harlen, O. G.; McLeish, T. C. B. *Macromolecules* **2001**, *34*, 2579.
(11) Colby, R. H.; Rubinstein, M. *Macromolecules* **1990**, *23*, 2753.
(12) Milner, S. T.; McLeish, T. C. B. *Macromolecules* **1997**, *30*, 2159.
(13) Frey, H.; Holter, D. *Acta Polym.* **1999**, *50*, 67.
(14) Biddlestone, F.; Goodwin, A. A.; Hay, J. N.; Mouledous, G. A. C. *Polymer* **1991**, *32*, 3119.
(15) Ferry, J. D. *Viscoelastic Properties of Polymers*; Wiley: New York, 1980.
(16) Milner, S. T.; McLeish, T. C. B.; Young, R. N.; Hakiki, A.; Johnson, J. M. *Macromolecules* **1998**, *31*, 9345.
(17) McLeish, T. C. B. *Macromolecules* **1988**, *21*, 1062.

MA011430S